Available online at www.sciencedirect.com
SCIENCE DIRECT®
Journal of Solid State Chemistry 178 (2005) 1601–1608
JOURNAL OF SOLID STATE CHEMISTRY
www.elsevier.com/locate/jssc

Neutron powder diffraction study of A_2BeF_4 (A = K, Rb, Cs): Structure refinement and analysis of background

Iván da Silva[a,*], Cristina González-Silgo[a], Javier González-Platas[a], Juan Rodríguez-Carvajal[b], María Luisa Martínez-Sarrión[c], Lourdes Mestres[c]

[a]*Departamento de Física Fundamental II, Universidad de La Laguna, Avda. Astrofísico Fco. Sánchez s/n, E-38204 La Laguna, Tenerife, Islas Canarias, Spain*
[b]*Laboratoire Léon Brillouin, C.E.A., Saclay, Grenoble, France*
[c]*Departamento de Química Inorgánica, Universidad de Barcelona, Diagonal 647, E-08028 Barcelona, Spain*

Received 14 January 2005; received in revised form 17 February 2005; accepted 27 February 2005

Abstract

The crystal structure of potassium, rubidium and caesium fluoroberyllates have been re-examined by neutron powder diffraction at room temperature and at 1.5 K. Previously, their structures, obtained from X-ray data, were described in the $Pn2_1a$ space group. However, the results obtained from Rietveld refinements, using powder neutron diffraction, at both temperatures, indicated that all structures are orthorhombic with space group *Pnma*. The known phase transition at high temperature is probably related to the appearance of a hexagonal pseudo-symmetry instead of the elimination of the mirror plane between the above mentioned orthorhombic space groups. A possible phase transition, at very low temperature, was discarded considering the stereochemical criteria concerning the structural stability of A_2BX_4 compounds. This was confirmed by thermal analysis. On the other hand, a modulated background has been detected in all samples during the refinements. This is compatible with the presence of an amorphous phase, coexisting with the crystalline phase, or with a disordered component within the main crystalline phase. Instead of using a polynomial function, the background was modelled by Fourier filtering improving the fit for all patterns. The radial distribution function (RDF) was obtained from the analysis of the calculated background and compared with the RDF from the average crystal structure. The advantages of neutron with respect to X-ray diffraction were evidenced for this type of compound with β-K_2SO_4-type structure.

Keywords: β-K_2SO_4 structure; Neutron power different

1. Introduction

We are interested in the large family of ferroelectrics compounds having the general formula A_2BX_4 with β-K_2SO_4 structure in the paraelectric phase (*Pnma* space group and $Z = 4$). The most widely studied compounds are K_2SeO_4, $(NH_4)_2SO_4$ and $(NH_4)_2BeF_4$, which are ferroelectrics at low temperature, however a number of physical properties related with the phase transition are strikingly different. A systematic analysis of A_2BX_4 compounds [1], reveals a correlation between the presence of low-temperature structural instabilities and some structural parameters; for instance: the bonding of the 11-coordinated cation (C-11), the ratio of ionic radii and the lattice parameters a/b. On the other hand, it is well established that the main structural condition to consider as potentially ferroelectric a polar crystal, is the presence of a maximum atomic displacement in the unit cell of about 1 Å along the polar direction with respect to the corresponding position in the paraelectric phase [2]. In addition, the largest of these atomic displacements from such a position must be significantly greater than about 0.1 Å of the r.m.s. amplitude of thermal displacement of that atom.

*Corresponding author. Fax: +34 922 318320.
E-mail address: idasilva@ull.es (I. da Silva).

0022-4596/$ - see front matter © 2005 Elsevier Inc. All rights reserved.
doi:10.1016/j.jssc.2005.02.026

In particular, potassium, rubidium and caesium fluoroberyllates, that were thought to belong to the $Pn2_1a$ polar space group at room temperature, are exceptional cases in this family of compounds. The difficulty to obtain good single crystals has limited the study of their dielectric and structural properties. Structural data date from the sixties [3,4]. Thermal analysis, standard X-ray powder diffraction and Raman scattering were carried out on K_2BeF_4 [5]: the high-temperature phase suggested that the low-temperature phase is ferroelectric. However, the structure determined by X-ray single crystal was described within the *Pnma* space group [6]. A poor refinement in $Pn2_1a$ was also obtained for Rb_2BeF_4 single crystals [7]. Both, Cs_2BeF_4 and Rb_2BeF_4, undergo a structural phase transition at high temperature but they have not been studied yet.

The aim of the present study is the re-determination of the space group and the accurate crystal structure of the three compounds: K_2BeF_4, Rb_2BeF_4 and Cs_2BeF_4 at room temperature and 1.5 K. The goal is to verify if these compounds are ferroelectrics or undergo phase transitions at low temperatures. The study at room and lower temperature will establish: (1) If all compounds have structures belonging to *Pnma* space group or to a less symmetric group. (2) The existence of polarization and, in the appropriate case, its direction. (3) The atom displacements from the corresponding paraelectric phase, in order to predict a possible high-temperature phase transition. (4) A comparison with other members of the A_2BX_4 family, in order to explain the origin of the structural instability in this type of structures. (5) The presence of a structural glass state or incompletely crystallized samples.

The advantages of neutrons for our study are: (1) Neutron powder diffraction is the best technique to refine crystal structures when single crystals are not available or present a domain structure (for instance, in ferroelectric phases). X-ray powder diffraction is prone to texture effects. (2) Relatively large sensitivity to beryllium and fluorine atoms. Neutron scattering leads to major accurate determination of their atomic and thermal parameters, allowing the analysis of dynamical aspects at different temperatures. (3) As a consequence, the diffuse background, arising from short-range correlations (Be–F and F–F) of site occupations or atomic positions, can be better treated than is the X-ray case.

2. Experimental and computational details

2.1. Experimental

The pure compounds A_2BeF_4, (A = K, Rb, and Cs) were obtained via the reaction:

$$BeF_2 + H_2F_2 + A_2CO_3 \rightarrow A_2BeF_4 + CO_2 + H_2O$$

BeF_2, H_2F_2 and A_2CO_3 were analytical grade. After completion of reaction, at pH = 7, the samples were slowly evaporated at room temperature. When A = K, as quickly as a precipitate appeared, it was filtered and the filtered liquid (pH = 7) was left to evaporate at room temperature. After a few days, a polycrystalline powder was obtained. The samples were not evaporated to dryness in order to avoid possible contamination of fluoroberyllates with residual impurities concentrated in the liquid. The polycrystalline powder was filtered and dried. All samples are stable.

SEM images were taken in a JEOL JSM 6300 at 20 kV of accelerating voltage, and a magnification of $\times 2000$. These images were used to check the refined parameters obtained from the calculated profile (grain size and shape) and samples quality (size dispersion, crystalline degree and grain morphology). Several differences were observed among the samples, which will be discussed below.

Thermal analyses were carried out on a Perkin-Elmer differential scanning calorimeter Pyris I-DSC. The samples were measured in the temperature range 98–773 K, with a warming rate of 10 K/min and a total scale sensitivity of 0.1 mW. The sample masses were 57.670, 11.460 and 26.270 mg for Cs_2BeF_4, K_2BeF_4 and Rb_2BeF_4, respectively. This analysis showed no thermal anomaly, so the samples were stable in this study.

The high-resolution neutron powder diffractometer 3T2, at the Orphée reactor of the Laboratoire Léon Brillouin (Saclay, France), was used for data collection with high direct space resolution ($\lambda = 1.2251$ Å, $Q_{max} = 9.2$ Å^{-1}). An helium cryostat was used to collect data at 1.5 K. No special sample environment was used to register the diffraction patterns at room temperature. Experimental details are given in Table 1.

2.2. Computational details

The program FullProf [8] was used for the Rietveld refinement of the six powder diffraction patterns. Peak search and visualisation were performed using the program WinPlotr [9]. The experimental profiles were always modelled using a Thompson-Cox-Hasting pseudo-Voigt profile shape function [10], with five adjustable parameters (U, V, W, X and Y); initial values were obtained from the instrumental resolution parameters. Peak asymmetry was also taken into account using two adjustable parameters [11]. After the preliminary refinements to fit the scale factor, zero point displacement, cell parameters and profile parameters, several cycles were performed to refine the atomic positions, isotropic (patterns measured at 1.5 K) and anisotropic (patterns measured at room temperature) thermal displacements. The starting values for the atomic positions were those of the β-K_2SO_4 structure, in the *Pnma* space group. Space group $Pn2_1a$ was also examined, without any

improvement, as we will discuss afterwards. Some additional details, and the final agreement factors, of the refinements are shown in Table 2. Fig. 1 shows the agreement between the calculated and observed profiles for K_2BeF_4 at two temperatures and two types of background models. In the next figures we show the results for the other compounds.

In the first stage of the refinement process, the background was adjusted by using of a polynomial function. But, due to the poor values obtained for the agreement factors and the modulated residuals that remained after the refinements, it was necessary to use another background modelling in order to improve the results. A Fourier filtering treatment was applied and we obtained clearly better results. This is an iterative procedure implemented in the program FULLPROF, so that the background at cycle "n" is calculated as follows:

$$\mathrm{Back}(n) = \mathrm{Back}(n-1) + \mathrm{Filtered}[y_{\mathrm{obs}} - y_{\mathrm{cal}}](n-1), \tag{1}$$

where Filtered[y_{obs}–y_{cal}] is a smoothed version of y_{obs}–y_{cal} [12] and the background for cycle $n = 1$ is that obtained from the polynomial modelling.

Table 1
Data collection

Radiation type	Neutron
Diffractometer	3T2, LLB
Wavelength (Å)	1.2251
2θ range	5–125
2θ step scan	0.05
Monochromator	Ge (335)
Sample environment	Cryostat (1.5 K)–None (298 K)

Although the previous treatment gives better results in the profile fitting procedure, it does not give us an idea about the cause of the residual modulation. That is why the residual was studied by performing an independent analysis, based in the assumption that the modulation appears from the presence of an amorphous phase in the samples or to short-range correlations from a disordered structure. The modulation of the background was still present at 1.5 K (Fig. 1c), so that thermal diffuse scattering (TDS) was discarded as being its origin. The RDF was obtained from the numerical approximation of the one-dimensional Fourier transform of the modulated residual coming from the non-crystalline scattering components using the following expression [13]:

$$d(r) = \frac{2}{\pi}\sum_{Q_{\min}}^{Q_{\max}} \frac{Q\sin\left(\frac{\pi Q}{Q_{\max}}\right)}{\left(\frac{\pi Q}{Q_{\max}}\right)\left[y_{\mathrm{obs}}(Q) - y_{\mathrm{cal}}(Q) - y_{\mathrm{bckg}}(Q)\right]\sin(Qr)\Delta Q}, \tag{2}$$

where $Q = 4\pi(\sin\theta/\lambda)$ and, $y_{obs}(Q)$, $y_{cal}(Q)$ and $y_{bckg}(Q)$ are the experimental profile, the calculated profile and the calculated background (with a polynomial modelling), respectively.

3. Results and discussion

The results of the adjustments were very similar in all compounds (see Table 2). Goodness of fit decreased at room temperature for all compounds, while other reliability factors and standard deviation were slightly improved at lower temperature. A good profile function adjustment is essential in order to obtain a more accurate structure and to be able to derive microstruc-

Table 2
Refinement strategies and results

Background	Fourier filter					
Excluded regions (2θ)	5–9					
Profile shape function	Thompson-Cox-Hasting pseudo-Voigt					
Structure refinement program	FULLPROF					
Weighting scheme	$w = 1/\sigma^2; \sigma^2 = y_i$					
Chemical formula	Cs_2BeF_4	Cs_2BeF_4	K_2BeF_4	K_2BeF_4	Rb_2BeF_4	Rb_2BeF_4
T (K)	1.5	RT	1.5	RT	1.5	RT
Space group	*Pnma*	*Pnma*	*Pnma*	*Pnma*	*Pnma*	*Pnma*
a (Å)	8.0929(1)	8.1550(2)	7.2527(3)	7.3005(3)	7.6409(1)	7.6900(2)
b (Å)	6.1047(1)	6.1675(1)	5.6272(2)	5.6886(3)	5.8253(1)	5.8892(2)
c (Å)	10.6475(1)	10.7499(2)	9.7969(4)	9.8817(5)	10.1528(2)	10.2437(3)
No. of reflections	933	933	721	721	808	808
No. of parameters refined	30	50	30	50	30	50
R_p	7.27	9.20	11.3	12.3	9.88	11.4
wR_p	7.99	8.53	12.2	11.8	11.6	12.9
$R(F^2)$	3.02	2.64	4.73	3.93	5.65	5.15
χ^2	2.87	1.64	3.65	2.80	11.4	8.41

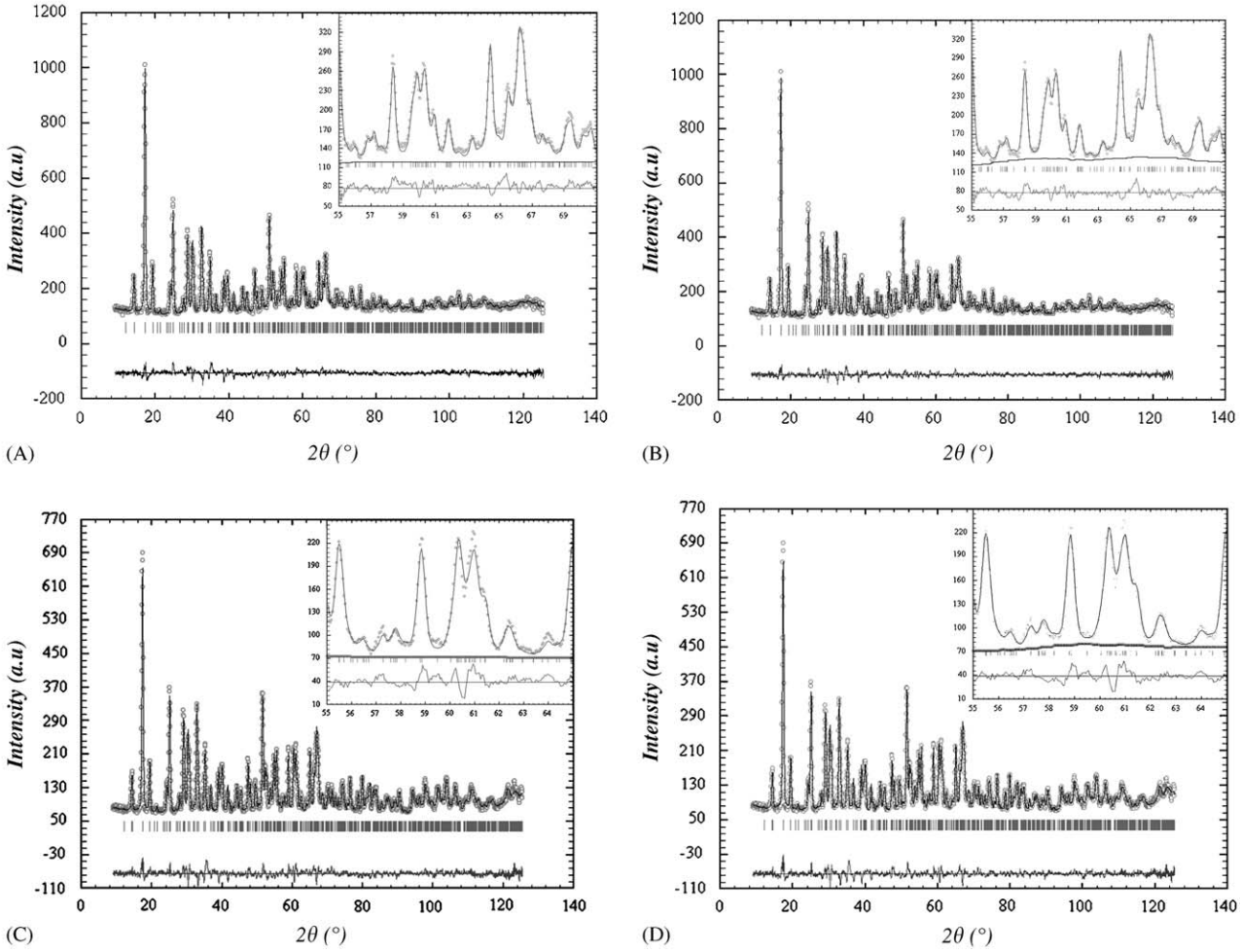

Fig. 1. Plot of the refinement results for K_2BeF_4, using (a, c) a polynomial background and (b, d) a Fourier filter (o experimental data, — calculated profile). Tick marks indicate the reflection positions and the difference yobs-ycalc is shown at the bottom. In (a) and (b) the patterns correspond to room temperature, while in (c) and (d) correspond to 1.5 K. The insets illustrate how the refinement is improved by the use of a Fourier filter to model the background.

tural and background effects. In this sense, in addition to the structure, all profile and background results have been physically interpreted too.

Parameters related to Gaussian contribution (given by U, V and W) were very similar in all compounds and they correspond well to the instrumental resolution function of 3T2. Only U and V parameters diminished slightly, at room temperature, while the other profile parameter was not temperature dependent. It is known that microstrain increases at lower temperature, then U and V temperature dependence is explained. Parameters related to Lorentzian contribution (X and Y) were approximately zero in all samples at two temperatures, excepting K_2BeF_4, in which the larger Y parameters (about 0.12 and 0.15 for low and room temperature, respectively) would indicate smaller domain or grain size. SEM microphotographs confirmed this difference: K_2BeF_4 shown smaller grain size (around 0.05 micrometer) with respect to the other fluoroberyllates. The increased peak width of two patterns also implied a diminution of peak asymmetry. More poorly results of Rb_2BeF_4 could be due to a more complex grain size distribution function, which was viewed in microphotographs.

In order to confirm the *Pnma* space group and to detect some structural instability, favouring a low-temperature phase transition, we have examined the following aspects at both temperatures:

(1) *Cell parameters*: Orthorhombic cells are similar to those calculated by other authors and cell parameters diminish normally at low temperature. Fig. 2 depicts values of a/c vs. a/b at room temperature and 1.5 K, showing a linear correlation. Fabry and Pérez-Mato [1] predicted this behaviour, in which the ionic radii ratio is a monotonically increasing function of a/b. The solid line indicates the loci fulfilling the condition $c = \sqrt{3}b$, and therefore corresponds to a perfect hexagonal metric of the lattice. The above-mentioned authors indicated that

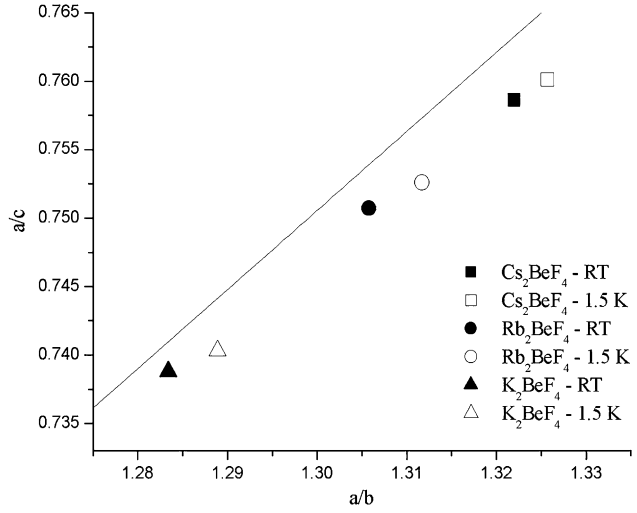

Fig. 2. Plot of the lattice parameter ratios a/c vs. a/b. The solid line corresponds to points with a hexagonal lattice metric.

the boundary between "unstable" and "stable" compounds would be situated around $a/b = 1.28$ and the unstable compounds would reveal a tendency to be situated above the solid line. A more recent stability diagram (González-Silgo et al., in preparation) based on A_2BX_4 pure compounds and their solid solutions (A = K, Rb, Cs, NH_4 and $BX_4 = SO_4$, SeO_4, BeF_4) confirmed both limits and it was found that all stable compounds satisfy the relation $a/c > 0.735$.

(2) Atomic coordinates and temperature factors, as well as the relevant distances together with the corresponding average distances and the cation bond valence sum (BVS) [14], are given in Tables 3 and 4, respectively. A different orientation, with respect to a hexagonal phase, around the c-axis of anions in the β-K_2SO_4 family was observed in several mixed crystals and some of them undergo low-temperature phase transition: $K_x(NH_4)_{2-x}SO_4$ [15], $K_x(NH_4)_{2-x}SeO_4$ [16] and $(NH_4)_2(SO_4)_x(BeF_4)_{1-x}$ [17]. The maximum and minimum values of the rotation angles are 3.96° in Cs_2BeF_4 and 1.96° in Rb_2BeF_4, at room temperature, respectively. Comparing with the other mentioned compounds, undergoing a low-temperature phase transition (10.5° in $(NH_4)_2BeF_4$ and 9.8° in $(NH_4)_2SO_4$), the anions are not significantly rotated. Another important parameter that distinguishes quite clearly between unstable and stable compounds is the ratio BV(C1)/BVS(C-11), where the cation with C-11 coordination must be underbonded (BVS less than 1) and the contribution of the shortest contact C1 to the BVS must be much bigger than the other contacts. The boundary can be situated around a value of 0.24 [1] and would be related with a major dispersion length around the C-11 cation due to the BX_4 group rotation (González-Silgo et al., in preparation). A value of this ratio, for our compounds, never exceeds 0.19 and the C-11 cations were quite overbonded without any particular short bond. Fig. 3 shows the C-9 and C-11 cation coordination of Rb_2BeF_4 at room temperature, which is very similar in all compounds.

(3) From the previous analysis, together with DSC results and the occurrence of similar structures at both temperatures, we concluded that these alkaline fluoroberyllates are stable at low temperature.

Table 3
Fractional atomic coordinates and isotropic temperature factors (for the 1.5 K case) or equivalent temperature factors (for the room temperature case)

	x	y	z	U (Å^2)
K_2BeF_4 (RT)				
K1	0.1638(7)	0.25	0.0942(9)	0.0219(9)
K2	−0.0106(11)	0.25	0.7000(7)	0.0309(15)
Be	0.2365(3)	0.25	0.4219(6)	0.0153(4)
F1	0.3051(5)	0.0277(5)	0.3446(5)	0.0341(8)
F2	0.0255(5)	0.25	0.4157(8)	0.0363(8)
F3	0.3065(9)	0.25	0.5640(6)	0.0312(12)
K_2BeF_4 (1.5 K)				
K1	0.1613(5)	0.25	0.0937(6)	0.0018(7)
K2	-0.0170(9)	0.25	0.6952(6)	0.0150(12)
Be	0.2352(3)	0.25	0.4227(4)	0.0063(4)
F1	0.3077(4)	0.0247(5)	0.3466(3)	0.0121(5)
F2	0.0210(4)	0.25	0.4136(4)	0.0093(6)
F3	0.3089(7)	0.25	0.5684(5)	0.0145(9)
Rb_2BeF_4 (RT)				
Rb1	0.1663(4)	0.25	0.0936(3)	0.0186(6)
Rb2	−0.0144(4)	0.25	0.6922(3)	0.0197(6)
Be	0.2406(3)	0.25	0.4175(4)	0.0137(4)
F1	0.3065(4)	0.0326(4)	0.3476(3)	0.0226(6)
F2	0.0397(4)	0.25	0.4123(5)	0.0219(6)
F3	0.3048(7)	0.25	0.5632(4)	0.0221(9)
Rb_2BeF_4 (1.5 K)				
Rb1	0.1626(2)	0.25	0.0937(2)	0.0007(3)
Rb2	−0.0132(3)	0.25	0.6901(3)	0.0044(4)
Be	0.2408(2)	0.25	0.4180(2)	0.0018(3)
F1	0.3117(3)	0.0317(3)	0.3495(2)	0.0030(3)
F2	0.0362(3)	0.25	0.4117(3)	0.0053(4)
F3	0.3057(4)	0.25	0.5637(3)	0.0056(6)
Cs_2BeF_4 (RT)				
Cs1	0.1651(3)	0.25	0.0943(3)	0.0209(5)
Cs2	−0.0153(3)	0.25	0.6893(3)	0.0203(6)
Be	0.2427(2)	0.25	0.4174(2)	0.0151(3)
F1	0.3119(3)	0.0452(3)	0.3500(2)	0.0270(5)
F2	0.0542(3)	0.25	0.4073(3)	0.0269(6)
F3	0.3076(4)	0.25	0.5541(3)	0.0270(8)
Cs_2BeF_4 (1.5 K)				
Cs1	0.1643(2)	0.25	0.0949(2)	0.0002(2)
Cs2	−0.0148(2)	0.25	0.6895(2)	0.0002(2)
Be	0.2435(2)	0.25	0.4169(2)	0.0034(2)
F1	0.3124(2)	0.0421(2)	0.3509(1)	0.0056(2)
F2	0.0524(2)	0.25	0.4087(2)	0.0060(3)
F3	0.3054(3)	0.25	0.5563(2)	0.0050(4)

Table 4
Interatomic distances (Å) and bond valence sums around the cations

	Cs_2BeF_4		K_2BeF_4		Rb_2BeF_4	
	1.5 K	RT	1.5 K	RT	1.5 K	RT
Be1–F1	1.554(2)	1.561(2)	1.563(3)	1.562(4)	1.548(2)	1.553(4)
Be1–F1, #4	1.554(2)	1.561(2)	1.563(3)	1.562(4)	1.548(2)	1.553(4)
Be1–F2	1.549(2)	1.542(3)	1.555(3)	1.542(4)	1.548(3)	1.545(4)
Be1–F3	1.567(3)	1.563(4)	1.523(6)	1.492(8)	1.560(4)	1.573(6)
Average distance	1.556(2)	1.557(3)	1.551(4)	1.540(5)	1.551(3)	1.556(5)
Bond valence sum	1.897	1.894	1.925	1.990	1.923	1.898
Cs11, K11, Rb11–F1, # 0	3.236(2)	3.254(4)	2.980(6)	2.967(8)	3.108(3)	3.094(4)
Cs11, K11, Rb11–F1, # 1	3.171(2)	3.201(3)	2.919(4)	2.971(6)	3.023(3)	3.108(4)
Cs11, K11, Rb11–F1, # 2	3.158(2)	3.201(3)	2.880(6)	2.935(8)	2.980(3)	3.027(4)
Cs11, K11, Rb11–F1, # 3	3.158(2)	3.201(3)	2.880(6)	2.935(8)	2.980(3)	3.027(4)
Cs11, K11, Rb11–F1, # 4	3.236(2)	3.254(4)	2.980(6)	2.967(8)	3.108(3)	3.094(4)
Cs11, K11, Rb11–F1, # 5	3.171(2)	3.201(3)	2.919(4)	2.971(6)	3.023(3)	3.108(4)
Cs11, K11, Rb11–F2, # 0	3.460(3)	3.485(5)	3.297(7)	3.33(1)	3.370(4)	3.407(6)
Cs11, K11, Rb11–F2, # 6	3.142(2)	3.174(3)	2.611(5)	2.643(6)	2.855(3)	2.872(4)
Cs11, K11, Rb11–F3, # 1	3.322(3)	3.322(4)	3.008(7)	3.038(9)	3.161(4)	3.213(6)
Cs11, K11, Rb11–F3, # 2	3.0897(4)	3.1219(7)	2.8329(8)	2.868(1)	2.9385(5)	2.9693(7)
Cs11, K11, Rb11–F3, # 7	3.0897(4)	3.1219(7)	2.8329(8)	2.868(1)	2.9385(5)	2.9693(7)
Average distance	3.203(2)	3.231(3)	2.922(5)	2.954(6)	3.044(3)	3.081(4)
Bond valence sum	1.136	1.050	0.965	0.883	1.068	0.970
Cs9, K9, Rb9–F1, # 8	3.027(2)	3.057(3)	2.646(6)	2.702(7)	2.838(3)	2.824(4)
Cs9, K9, Rb9–F1, # 9	2.969(2)	3.008(3)	2.625(6)	2.607(7)	2.772(3)	2.804(4)
Cs9, K9, Rb9–F1, # 10	3.027(2)	3.057(3)	2.646(6)	2.702(7)	2.838(3)	2.824(4)
Cs9, K9, Rb9–F1, # 11	2.969(2)	3.008(3)	2.625(6)	2.607(7)	2.772(3)	2.804(4)
Cs9, K9, Rb9–F2, # 0	3.039(3)	3.083(5)	2.773(7)	2.82(1)	2.850(4)	2.897(6)
Cs9, K9, Rb9–F2, # 12	3.241(1)	3.270(2)	3.010(3)	3.067(4)	3.096(1)	3.139(2)
Cs9, K9, Rb9–F2, # 8	3.241(1)	3.270(2)	3.010(3)	3.067(4)	3.096(1)	3.139(2)
Cs9, K9, Rb9–F3, # 0	2.953(3)	3.008(4)	2.672(7)	2.68(1)	2.754(4)	2.789(6)
Cs9, K9, Rb9–F3, # 13	3.073(3)	3.113(4)	2.638(7)	2.687(9)	2.858(4)	2.865(6)
Average distance	3.060(2)	3.097(3)	2.738(6)	2.771(7)	2.875(3)	2.898(4)
Bond valence sum	1.369	1.235	1.279	1.192	1.370	1.293

Symmetry codes:# 0: X, Y, Z; # 1: X–0.5, $-Y$+0.5, -Z+0.5; # 2: $-X$+0.5, $-Y$, Z–0.5.
3: $-X$+0.5, Y+0.5, Z–0.5; # 4: X, $-Y$+0.5, Z; # 5: X–0.5, Y, $-Z$+0.5.
6: X+0.5, $-Y$+0.5, -Z+0.5; # 7: $-X$+0.5, $-Y$+1, Z–0.5; # 8: $-X$, Y+0.5, $-Z$+1.
9: $-X$+0.5, $-Y$, Z+0.5; # 10: $-X$, $-Y$, $-Z$+1; # 11: $-X$+0.5, Y+0.5, Z+0.5.
12: $-X$, Y–0.5, $-Z$+1; # 13: X–0.5, $-Y$+0.5, $-Z$+1.5.

However, from this study, it was not possible to establish unambiguously the space group (polar or non-polar). A consequence of the mirror plane, in *Pnma*, is the restriction of the dipoles to this plane. The inversion centre causes all dipoles within the entire unit cell to cancel above T_c. Removing the mirror plane ($Pnma \rightarrow Pn2_1a$) results in displacements Δy of cations along the polar direction, from the plane containing the effective negative point charge associated with the anion BeF_4^{-2}. The calculated displacements in non-centrosymmetric structures ($Pn2_1a$ in our case), at room temperature, were: $\Delta y(K_2BeF_4) = 0.13$ Å, $\Delta y(Rb_2BeF_4) = 0.09$ Å, $\Delta y(Cs_2BeF_4) = 0.05$ Å. Although they are longer than isotropic thermal parameters, they are too short in order to expect a high-temperature transition to the *Pnma* space group with T_c above 500 K (T_c is calculated according to the equation: $\Delta y = KT_c^2$, [18]). However, values closer to the experimental transition temperatures were obtained making calculations in *Pmcn* (*Pnma*) space group (having displacements, parallel to axes contained in the mirror plane) with respect to the $P6_3/mmc$ space group (model Apex with five special sites [19]). Then, it is more probable a hexagonal phase at high temperature. At present, we are measuring these compounds at high temperature and all patterns are well indexed in hexagonal cells, but a more complete study by neutron diffraction is required in order to refine the crystal structures.

(4) *Background interpretation:* The different results obtained in the refinement by changing the background modelling can be seen in Fig. 1. There, it is detailed how the modulation in the residuals disappears when the background is treated by using the Fourier filtering technique (Figs. 1b and d) instead of the

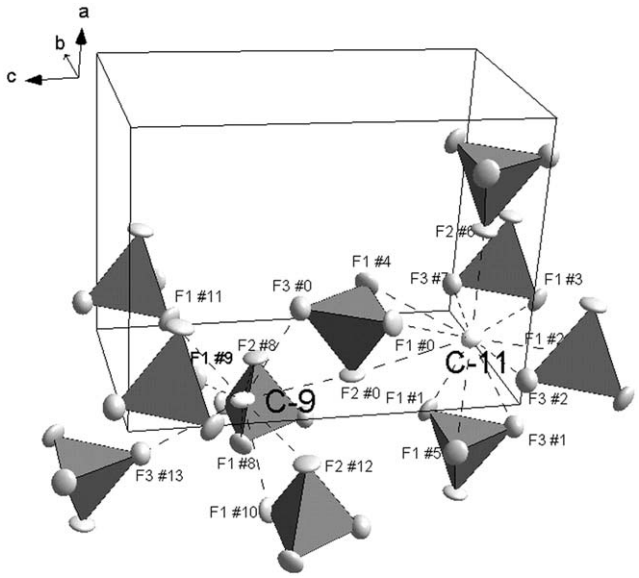

Fig. 3. Arrangement of the closest neighbours BeF_4 tetrahedra to 9 and 11-coordinated cations (C-9 and C-11) in the structure. The figure depicts the case of Rb_2BeF_4 at room temperature. The thermal ellipsoids are drawn at 70% probability.

polynomial modelling (Figs. 1a and c). Some of the consequences in the refinement were the following: (1) an improvement in the reliability indices (e.g. χ^2 and $R(F^2)$ improve by 30% and 50%, respectively) and (2) some thermal parameters had no longer negative values, as they had using a polynomial background. Fig. 4 illustrates the result of the analysis of the residual wavy background according to Eq. (2) for the Cs_2BeF_4 (a) at room temperature and (b) at 1.5 K. It shows the RDF, obtained from Eq. (2), compared to the distribution of the different kinds of interatomic distances, for the ideal crystalline phase. It can be seen how the positions of the first two maximums of the RDF are very close to the Be–F and F–F interatomic distances. A similar agreement was obtained for all the three samples and for both room temperature and 1.5 K. The major dispersion at longer interatomic distances made the RDF maximums to be not well defined, making it difficult to assign each maximum with a determined kind of interatomic contact. In order to obtain more quantitative results from RDF, it would be necessary to obtain a more precise measurement of the intensities and additional measurements in order to put the intensities in absolute values (barns). This was not possible in the allocated beam time. However, these qualitative results justify the use of the Fourier filtering technique instead of the polynomial function. Moreover, we have obtained a strong indication that the observed background probably comes from correlated rotational disorder of BeF_4 tetrahedrons. This can be seen in the broader second peak of the RDF at RT compared

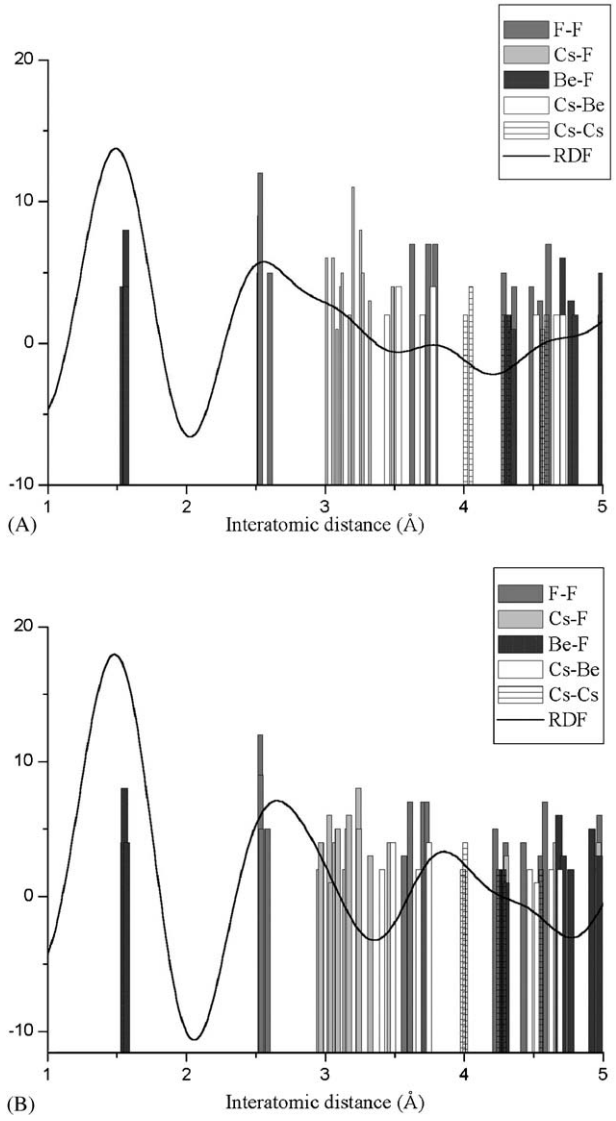

Fig. 4. Representation of the radial distribution function (RDF, solid line), obtained from the analysis of the background (see text), and its comparison with the interatomic distances (columns) obtained from the refinement at (a) room temperature and (b) 1.5 K, for the Cs_2BeF_4 case.

with the RDF at 1.5 K. For instance, Be–F and F–F bond lengths, corresponding to the tetrahedrons, were very similar for the three compounds at both 1.5 K and room temperature. Also, there is a small diminution of other bond lengths at 1.5 K, due to the cell contraction. Moreover, interatomic distances containing an alkaline cation were longer for Cs_2BeF_4 and shorter for K_2BeF_4.

4. Conclusions

This work presents the second neutron diffraction study performed in fluoroberyllates with β-K_2SO_4 structure (firstly the ammonium fluoroberyllate was

studied [20]) and it shows the adequacy of this technique for this type of compounds. The overall study provides significant evidence of the advantages of the neutron powder diffraction technique for solving/refining the crystal structure of these materials. This is so because single crystal cannot be obtained and because X-ray radiation is too much destructive for these very crumbly and incompletely crystallised samples. Hence the problem of obtaining good results in previous studies. Refinement of crystal structures in *Pnma* space group, at room temperature and 1.5 K, together with a bond valence analysis and the occurrence of some structural correlations, indicated that all structures are stables at low temperature. Because of the no existence of significant displacements between refined structures in $Pn2_1a$ and *Pnma* space groups, we cannot expect that none compound acquire the non-polar configuration above 500 K. However, longer displacements calculated from the β-K_2SO_4 phase to the hexagonal α-K_2SO_4 phase makes these compounds to be considered as having a high probability of exhibiting a phase transition at high temperature from *Pnma* to the hexagonal phase. Otherwise, the agreement between calculated and experimental patterns is better, for all compounds and at both temperatures, when a Fourier filter is used to model the background. This can be justified because from the modulated residues has been calculated the RDF for each fluoroberyllate compound, due to the coexistence of an amorphous phase with the crystalline structure.

Acknowledgments

The authors are grateful for the allocation of beam time at the Laboratoire Léon Brillouin (CEA-CNRS), Saclay, France.

References

[1] J. Fabry, J.M. Pérez-Mato, Phase Transition 49 (1994) 193–229.
[2] S.C. Abrahams, Acta Crystallogr. B 44 (1988) 585–595.
[3] D.Yu. Pushcharovskii, A. Ganem, E.A. Pobedimskaya, N.V. Belov, Sov. Phys.-Crystallogr. 13 (1969) 930–932.
[4] N.M. Mustafaev, V.V. Ilyukhin, N.V. Belov, Sov. Phys.-Crystallogr. 10 (1966) 676–683.
[5] X. Solans, C. González-Silgo, T. Calvet, C. Ruiz-Pérez, M.L. Martínez-Sarrión, L. Mestres, Phys. Rev. B 57 (1998) 5122–5125.
[6] A. Onodera, T. Sawada, Y. Kawamura, T. Takama, M. Fujita, H. Yamashita, J. Korean Phys. Soc. 32 (1998) 73–76.
[7] A. Onodera, I. Takahashi, S. Ishii, Shiozaki, Jpn. J. Appl. Phys. 24 (1985) 591–593.
[8] J. Rodríguez-Carvajal, Fullprof.2k, Versión 1.9c, Laboratoire Léon Brillouin, Paris, France, 2001.
[9] T. Roisnel, J. Rodríguez-Carvajal, WinPlotr, a Graphic Tool for Powder Diffraction (2001).
[10] P. Thompson, D.E. Cox, J.B. Hastings, J. Appl. Cryst. 20 (1987) 79–83.
[11] J.F. Berar, G. Baldinozzi, J. Appl. Cryst. 26 (1993) 128–129.
[12] W. Press, S. Teukolsky, W. Vetterling, B. Flannery, Numerical Recipes, Cambridge, 1992.
[13] R.A.Young, The Rietveld Method, Oxford Science Publications, Oxford, 1991.
[14] N.E. Brese, M. O'Keeffe, Acta Crystallogr. B 47 (1991) 192–197.
[15] C. González-Silgo, X. Solans, C. Ruiz-Pérez, M.L. Martínez-Sarrión, L. Mestres, E. Bocanegra, J. Phys.: Condens. Matter 9 (1997) 2657–2669.
[16] X. Solans, C. Ruiz-Pérez, C. González-Silgo, L. Mestres, M.L. Martínez-Sarrión, E. Bocanegra, J. Phys.: Condens Matter 10 (1998) 5245–5253.
[17] C. González-Silgo, C. Ruiz-Pérez, Ferroelectrics 175 (1996) 207–218.
[18] S.C. Abrahams, S.K. Kurtz, P.B. Jamieson, Phys. Rev. 172 (1968) 551–555.
[19] J.A. McGinnety, Acta Crystallogr. B 28 (1972) 2845–2852.
[20] R.C. Srivastava, W.T. Klooster, T.F. Koetzle, Acta Crystallogr. B 55 (1999) 17–23.